ACS APPLIED MATERIALS & INTERFACES

www.acsami.org

Research Article

Discovery of Clustered-P1 Borophene and Its Application as the Lightest High-Performance Transistor

Sirsha Guha, Arnab Kabiraj, and Santanu Mahapatra*

Cite This: https://doi.org/10.1021/acsami.2c20055

Read Online

ACCESS | Metrics & More | Article Recommendations | Supporting Information

ABSTRACT: The two-dimensional network of boron atoms (borophene) has attracted attention for its ultralow molar mass and remarkable polymorphism. Synthesized polymorphs of borophene (striped, β_{12}, χ_3, and honeycomb), so far, are all found to be metallic. Employing a genetic algorithm-based structure searching technique, here we discover an allotrope, clustered-P1, which is located very close to the global energy minimum. Clustered-P1 exhibits a bulk silicon-like band gap (1.08 eV) with symmetric effective masses (~0.2 m_0) for electrons and holes along the transport direction. Phonon dispersion and beyond room-temperature *ab initio* molecular dynamics studies further confirm its excellent dynamic and structural stability. Since two-dimensional semiconductors are promising silicon alternatives for complementary metal-oxide semiconductor (CMOS) technology extension, we further investigate the characteristics of clustered-P1-based transistors using self-consistent quantum transport models for channel lengths of 10−3 nm. The performance of these devices has been found to be balanced for p- and n-type transistors and meets the requirements of the International Roadmap for Devices and Systems (IRDS). Our study may aid in the experimental realization of the lightest high-performance transistor.

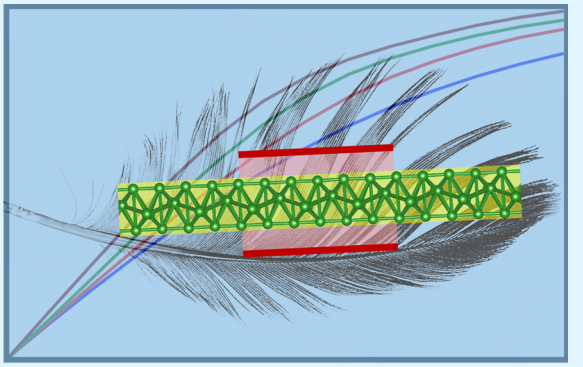

KEYWORDS: *2D materials, borophene, genetic algorithm, density functional theory, molecular dynamics, quantum transport, transistors*

INTRODUCTION

The chemical bonding between boron atoms is more complex than between carbon atoms since boron is located to the left of carbon in the periodic table and thus possesses a shorter covalent radius. Unlike carbon, which favors a two-dimensional (2D) layered structure (graphite) in its bulk form, B_{12} icosahedral cages are the building blocks in bulk boron and many other boron compounds.[1] As a result, though the possibility of a 2D atomic network of boron (borophene) was predicted computationally in 2007,[2] its experimental realization happened only in 2015.[3] Again, in contrast to graphene, in this study and successive experiments,[4] 2D networks of boron atoms are found in different polymorphs. Interestingly, all of these polymorphs (striped, β_{12}, χ_3, and honeycomb)[3−5] are found to be metallic, whereas bulk boron is semiconducting in nature. Therefore, the search for a semiconducting 2D phase of boron has become a natural scientific quest. Meanwhile, a large variety of borophenes have been predicted computationally, some of which can even host tilted-Dirac Fermion[6,7] and magnetic order.[8] The ultralow molar mass and metallic nature of borophene have prompted a wide range of electrochemical applications, e.g., alkali-metal-ion batteries, hydrogen storage, supercapacitor, and catalytic reaction.[9,10]

Since the performance of ultrascaled silicon-based transistors has reached its bottleneck,[11] the exploration of two-dimensional (2D) materials, which promise to deliver ultimate electrostatic integrity, has become necessary in the semiconductor industry as a replacement for silicon.[12] To date, more than a dozen 2D semiconductors (e.g., germanane,[13] phosphorene,[14] tellurene,[15] etc.) have been explored experimentally for transistor channel applications. However, the 2D material space is infinite, and experimental efforts can cover only a small fraction of it. With the advances of computational science and technology, *in silico* discovery of appropriate transistor materials has gained popularity in exploring this gigantic material space.[16,17] Discovery of a semiconducting phase of borophene, with a silicon-like band gap yet lower effective mass, with good thermodynamic, structural, and dynamic stability is thus important for the practical application of borophene as a transistor channel. Semiconducting phases of borophene reported in recent studies[18,19] exhibit small band gaps and, therefore, may not be good options for transistor channels.

Received: November 9, 2022
Accepted: December 29, 2022

Table 1. Comparison of Noteworthy Borophene Allotropes

polymorph	$E_{tot\text{-}PBE}$(eV/atom)	$E_{tot\text{-}HSE}$(eV/atom)	$E_{g\text{-}PBE}$ (eV)	$E_{g\text{-}HSE}$ (eV)	a (Å)	b (Å)	t (Å)	α (deg)	β (deg)	γ (deg)
α	−6.306	−6.943	metal	metal	4.47	4.47	0	90	90	81.92
χ_3	−6.270	−6.900	metal	metal	4.46	4.46	0	90	90	37.92
β_{12}	−6.259	−6.905	metal	metal	5.07	2.93	0	90	90	90
striped	−6.212	−6.849	metal	metal	1.61	2.87	0.9	90	90	90
sliced	−6.365	−7.043	metal	metal	3.18	2.84	3.06	90	90	116.57
8-*Pmmn*	−6.352	−7.027	semimetal	semimetal	3.26	4.52	2.19	90	90	90
clustered-P1	−6.300	−6.973	0.543	1.084	3.17	4.49	2.52	90	90	93.94
B_8-1*	−6.207	−6.857	0.210	0.591						
B_{12}-1*	−6.208	−6.860	0.560	0.880						
B_{12}-2*	−6.186	−6.832	0.539	0.776						

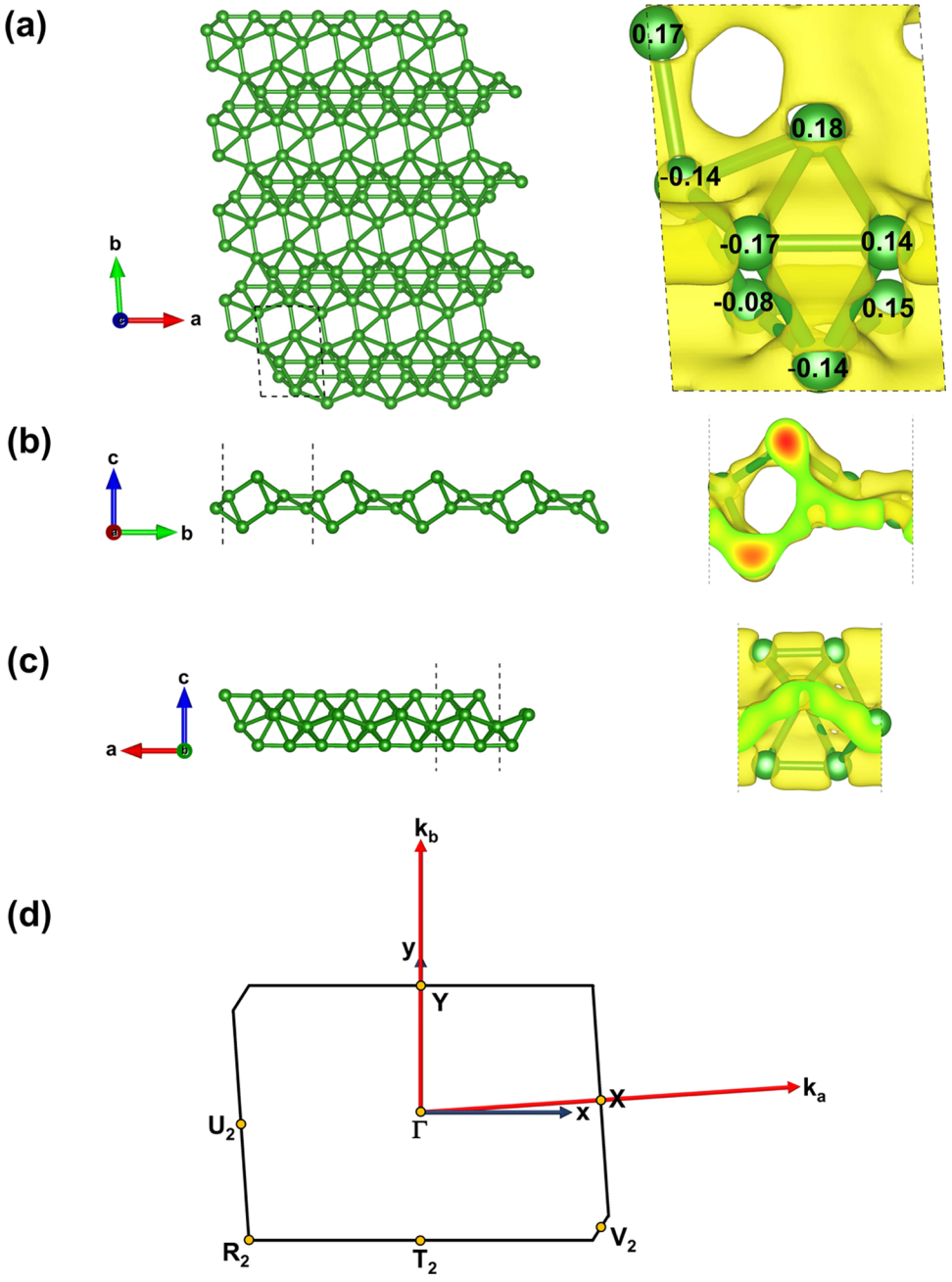

Figure 1. Structure of clustered-P1 borophene. (a) Top and (b, c) side views of CP1 borophene, along with its charge density. The Bader charges are mentioned for each atom in the top view (a). (d) First Brillouin zone and symmetry points of the CP1 phase. The dotted lines represent the unit cell boundary. The charge density has been calculated with HSE.

https://doi.org/10.1021/acsami.2c20055
ACS Appl. Mater. Interfaces XXXX, XXX, XXX−XXX

In this work, using a genetic algorithm-based structure searching technique, we discover a new allotrope of 2D boron, which we name clustered-P1 (CP1). This new allotrope is found to be located very close (0.07 eV/atom higher) to the global minimum of the energy surface, which signifies good thermodynamic stability. CP1 borophene exhibits a band gap of 1.08 eV, which is very similar to that of bulk silicon, but it inherits lower and symmetric effective masses (~0.2 m_0) for electrons and holes along the transport direction. Additional evidence of its outstanding dynamic and structural stability comes from studies of phonon dispersion and beyond room-temperature *ab initio* molecular dynamics. We further investigate the characteristics of CP1-based transistors using self-consistent quantum transport models, which were absent in previous studies.[18,19] Performance of these devices has been found to meet the requirements of the International Roadmap for Devices and Systems (IRDS). Even a 3 nm channel device is shown to deliver a 10^4 ON−OFF current ratio. Our research could help with the experimental development of the lightest, high-performance transistor made of any 2D material yet.

RESULTS AND DISCUSSION

Discovery of Clustered-P1 Borophene. We begin the study with a first-principles-based search of the 2D boron space using an evolutionary algorithm.[6,20−24] Similar studies have previously discovered novel borophene phases hosting Dirac fermions[6] and low to moderate band gaps.[18] However, the total energies of the semiconducting phases are much higher than the global minimum, which signifies the low thermodynamic stability of the predicted semiconducting allotropes. Our evolutionary algorithm-powered structure searching yields a unique semiconducting borophene phase, not reported previously, which also exhibits a total energy close to the global minimum of all borophene phases. Fine details of the structure searching process can be found in the Methods section.

The total energies, band gaps, and structural parameters of some noteworthy borophene allotropes found in our search are listed in Table 1. The 2D space is defined in such a way that it does not allow polymorphs thicker than 3 Å to survive, and this definition was effective in finding all major experimentally synthesized and computationally predicted phases. A general trend of thicker borophenes being significantly more stable than their flat (zero-thickness) or nearly flat counterparts is observed. Among the flat or near-flat polymorphs, our search expectedly finds the α phase to be the most stable.[2,25] Also, the experimentally synthesized flat χ_3 and β_{12} phases and nearly flat striped phases are found.[3,4] However, the search is unable to find the experimentally synthesized honeycomb borophene phase since its freestanding form is extremely unstable compared to the other low-energy phases mentioned in Table 1.[5,24] It is also well known that this phase can only stabilize after adsorbing a significant amount of charge from its substrate.[24] The allotrope at the global energy minimum expectedly turns out to be a 3 Å thick slice of bulk boron, which we call sliced borophene. The top and side views of this structure are shown in Figure S1, while its crystal structure information is provided in Table S1. We also found the famous semimetallic 8-*Pmmn* borophene, which hosts a tilted-Dirac cone in its band structure, and we note that it is extremely close (0.016 eV/atom higher according to Heyd−Scuseria−Ernzerhof (HSE) hybrid exchange-correlation (XC) functional) to the global minimum in terms of total energy. Energetically a little higher (0.07 eV/atom according to HSE XC), we find the semiconducting clustered-P1 (CP1) phase. We also tabulate the three most stable semiconducting phases (marked by *) found by Zhang et al.[18] with their total energies and band gaps. It is evident that the CP1 phase is far more energetically stable than these three phases, and it also boasts a significantly higher band gap, similar to that of bulk silicon.

Electronic Structure and Stability of CP1 Borophene. The crystal structure information of the CP1 phase is given in Table S2, while its top and side views, along with the charge densities and Bader charges, are depicted in Figure 1a−c. The CP1 borophene exists in a near-rectangular unit cell, where the angle between the in-plane lattice vectors is 93.94°, making it technically a triclinic P1 cell. Clear boron clustering and intercluster regions can be identified from the crystal structure (Figures 1a and S2). Also, at the intercluster region, a large hole can be noticed in the charge density from the top view. The charges seem to be mostly spread around the bonds rather than the atoms, indicating the presence of highly covalent bonds in the material. However, a closer look reveals that the four clustered boron atoms in the unit cell each show nearest-neighbor coordination of 5, while the other four intercluster boron atoms each exhibit larger coordination of 7 (Figure S2). This is indeed remarkable, considering each boron atom possesses only three valence electrons. To gain further insights into the peculiar bonding of CP1 borophene, we apply a density-derived electrostatic and chemical (DDEC6) charge partitioning scheme on the HSE-calculated charge density. This method unveils and adequately quantifies the bond order of all of the bonds of the material, which is summarized in Figure S2. The total bond order of each atom, i.e., the sum of the bond orders of all of the bonds the atom has formed, is always close to 3. We observe that the interbonding between the four boron atoms constituting the cluster shows a bond order of nearly 1. However, all of the other nearest-neighbor bonds in the material show bond order $\leq$ 0.56. The bond order stoops as low as 0.14 for the longest bond of the intercluster region, which is marked as a hole in the charge density shown in Figure 1a. The low bond order of these bonds can be explained by the fact that at least one of the atoms forming the bond possesses an extremely high coordination of 7 and therefore contributes much less charge to each bond when compared to the intracluster region. Therefore, except for the cluster region, all bonds of the materials are severely electron-deficient. This multicenter bonding phenomenon somewhat resembles the well-known three-center two-electron (3c-2e) bond but can be considered a more extreme form of electron-deficient bonding, giving rise to this unique borophene phase. However, the presence of electron-deficient bonds does not undermine the material's stability, as we will show next. The presence of electron-deficient bonds is also common in other borophene phases as well, and the ability of boron to form stable electron-deficient bonds is probably the reason for its rich polymorphism in 2D. The boron atoms of synthesized borophene phases χ_3, β_{12}, and striped shows nearest-neighbor coordination of 4−6. Interestingly, all of the boron atoms of the honeycomb phase show coordination of 3, yet the phase is highly thermodynamically unstable and only stabilizes upon electron adsorption.[5,24]

Unsurprisingly, the material turns out to be purely nonmagnetic. The first Brillouin zone (BZ) of the material is depicted in Figure 1d, where we also highlight the high-symmetry points of this rather "asymmetric" material. We also

https://doi.org/10.1021/acsami.2c20055
ACS Appl. Mater. Interfaces XXXX, XXX, XXX−XXX

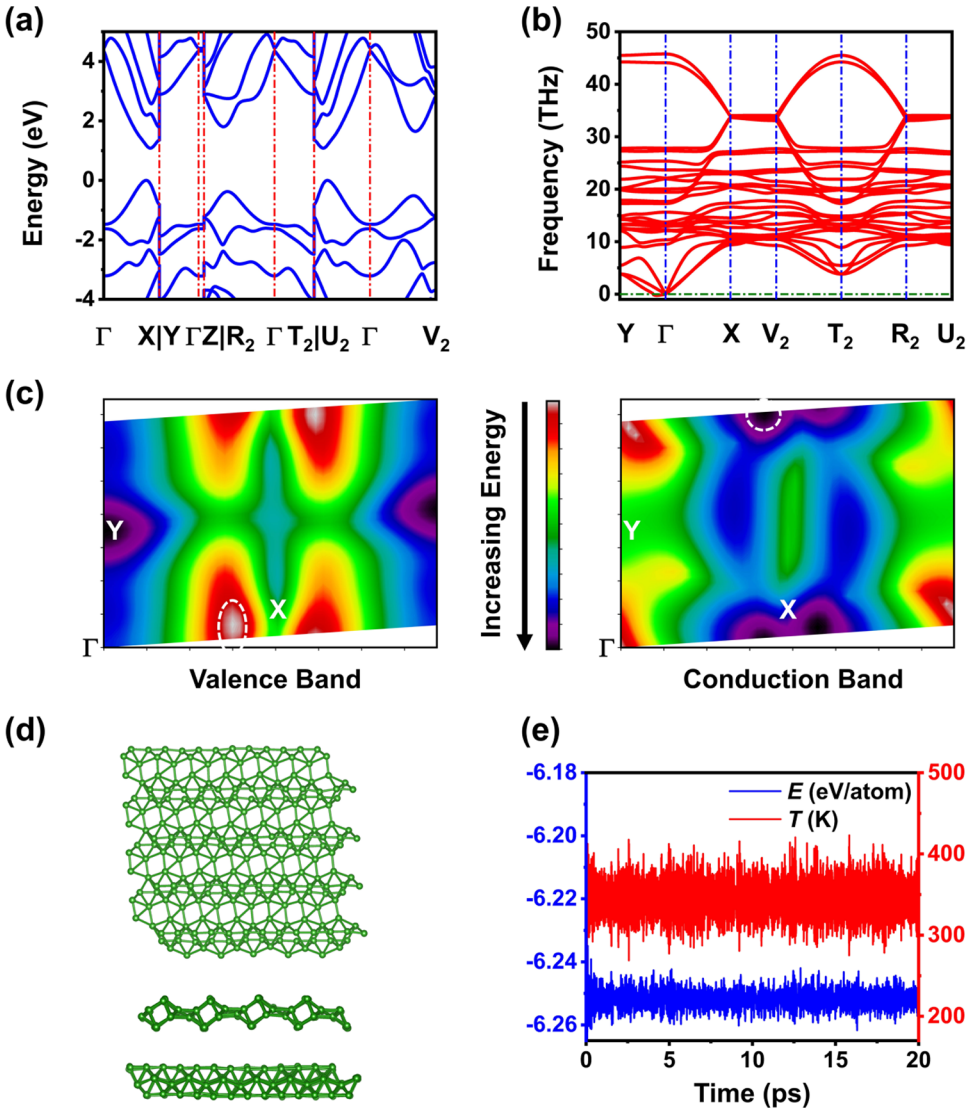

Figure 2. Electronic structure and stability of clustered-P1 borophene. (a) Electronic and (b) phonon band dispersions. (c) Contour plot of the valence and conduction band. The VBM and CBM are highlighted with a white dotted ellipse and circle. (d) CP1 structure after spending 20 ps at 350 K. (e) Total energy and temperature variation with time for AIMD. The imaginary frequencies in the phonon spectrum are represented as negative frequencies.

observed that forcefully making the cell perfectly rectangular yields an energetically slightly less stable but dynamically quite unstable phase.

It is well-known that local and semilocal DFT, such as the one employing Perdew–Burke–Ernzerhof (PBE) XC functional, severely underestimates a material's band gap compared to experimental findings. On the other hand, hybrid functionals, especially HSE06, have been demonstrated to predict band gaps accurately, albeit being computationally extremely expensive.[26] For our purpose, accurate prediction of electronic properties like band gap and effective mass is essential as these ultimately decide the electrical properties of the potential transistor. Therefore, we have calculated the electronic properties with HSE whenever possible (see Methods for details).

The HSE-calculated band structure is plotted in Figure 2a. The band gap is slightly indirect, and both valence band maximum (VBM) and conduction band minimum (CBM) are situated closer to the X point on the line joining the Γ and the X point. The total and orbital-resolved density of states is plotted in Figure S3. Strong hybridization between the s and p orbitals is observed, with the p_z orbital contributing most states near the VBM and CBM. The PBE-calculated phonon band structure is plotted in Figure 2b. The phonon spectrum effectively does not show any imaginary frequencies (except for an acoustic branch near the Γ point protruding negligibly into the imaginary region because of well-known numerical problems), indicating high dynamic stability of the material. The HSE-calculated contour plots of the valence band and conduction band are shown in Figure 2c. While the VBM appears rather elliptical, the CBM appears much more circular. Confirming this, the HSE-calculated hole effective mass in the x and y-directions turn out to be $m_{hx} = 0.217\ m_0$ and $m_{hy} = 0.622\ m_0$, where m_0 is the mass of a stationary electron. The electron effective mass in both directions is found to be $m_e = 0.194 m_0$. It is worth mentioning that while calculating the effective masses, we assumed the $\boldsymbol{k}_a$ and $\boldsymbol{k}_b$ vectors to be orthogonal, while this is not the case in reality (Figure 1d). The angle between them is 86.03°, which we reasonably approximate to 90° for the ease of calculations. The in-plane

https://doi.org/10.1021/acsami.2c20055
ACS Appl. Mater. Interfaces XXXX, XXX, XXX−XXX

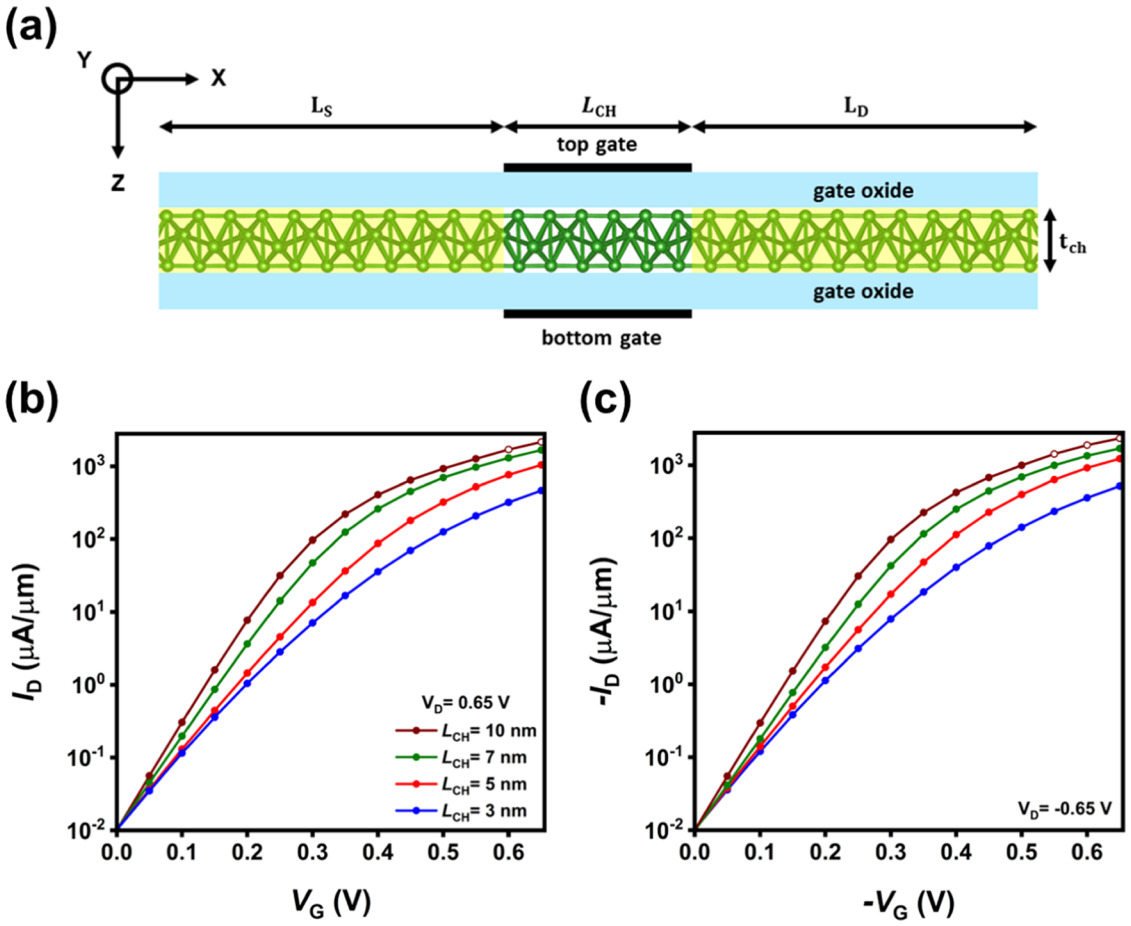

Figure 3. Device schematic and transfer characteristics. (a) Schematic of the cross-sectional (x−z plane) view of the simulated MOSFET. The channel is undoped, whereas the source and drain regions (shaded) are uniformly doped. Transfer characteristics ($I_D - V_G$) of (b) n-type and (c) p-type MOSFETs at a drain bias of $|V_D|$ = 0.65 V for L_{CH} = 10−3 nm.

dielectric constant is also highly anisotropic, with the PBE-calculated values k_x = 5.19 and k_y = 2.74. The HSE-determined electron affinity of the material is χ = 4.9 eV.

For transistor applications, testing the material's thermal stability is essential, as we expect the device to work at room temperature and beyond and anticipate significant heating during high-frequency operations. To ensure suitable thermal stability, we perform *ab initio* molecular dynamics (AIMD) simulation where the material is subjected to a 350 K temperature for 20 ps. Figure 2d shows the top and side views of the CP1 structure after being exposed to 350 K for 20 ps, where absolutely no damage or structural changes can be observed, establishing excellent thermal stability of this polymorph. Note that despite most of the bonds constituting the material being highly electron-deficient, they indeed are capable of a strong cohesion, enough to hold the material together beyond room temperature firmly. Figure 2e plots the total energy and temperature over time, and no drifts are observed in these quantities as well. Supporting Video shows the trajectory of the atoms during the AIMD simulation.

It is possible to predict the ideal synthesis conditions of borophenes using computational techniques like DFT, MD, or Monte Carlo (MC) simulations, but these studies can be extremely expensive.[27−29] An accurate prediction of the exact synthesis conditions for CP1 borophene is out of the scope of this work and can be taken up as a separate follow-up study. There is, however, a valuable hint about the type of substrate to be used for the possible synthesis of this phase. Like other synthesized borophenes, CP1 exhibits electron-deficient bonds. Although the honeycomb borophene theoretically houses electron-content bonds, the material requires outside electrons to stabilize, and it has only been synthesized on an active electron-donating Al(111) surface.[5] Judging by this trend, we expect the CP1 borophene phase to require relatively passive substrates, such as Ag/Au(111), to be synthesized on, with the metal surface providing the necessary passivation for the hybridized bonds.[27]

Quantum Transport Modeling of the CP1 Borophene Transistor. Having explored CP1 borophene's material properties thoroughly, we identify this material as ideal for application in next-generation metal-oxide-semiconductor field-effect transistors (MOSFETs). The silicon-like band gap but lower effective masses suggest that the devices made from CP1 borophene can exhibit high ON current with fast switching.

The combined DFT-NEGF (non-equilibrium Green's function)-based methodology, such as the one implemented in the QuantumATK package,[30] has become prominent for exploring 2D material-based transistor characteristics.[31−34] However, this methodology can become computationally prohibitively expensive when employed with hybrid functionals such as HSE. Apart from that, the Brillouin zone of clustered-P1 borophene, shown in Figure 1d, is not orthogonal, and QuantumATK is not adaptable to such crystal structures.

https://doi.org/10.1021/acsami.2c20055
ACS Appl. Mater. Interfaces XXXX, XXX, XXX−XXX

Table 2. Figures of Merit of Clustered-P1 Borophene MOSFETs

parameter	n-MOSFET				p-MOSFET			
L_{CH} (nm)	10	7	5	3	10	7	5	3
I_{ON}(mA/μm)	2.16	1.68	1.05	0.47	2.35	1.71	1.23	0.52
PDP (aJ/μm)		121	95	74		126	97	75
τ (fs)		111	140	243		114	121	222
SS (mV/dec)	67	77	88	93	67	80	87	92

Therefore, the DFT-NEGF-based methodology is not fit for our study. From the electronic band structure (Figure 2a), we do not observe any degeneracy at conduction or valence band extrema. The CBM exhibits isotropic dispersion; however, at the VBM, the dispersion is anisotropic. The material possesses a large band gap (1.08 eV), and thus for carrier transport through n- or p-type MOSFETs, we do not expect any interaction between conduction and valence bands. Keeping these distinct features of the electronic structure in mind, we have chosen a single band effective mass Hamiltonian separately for n- and p-type MOSFETs as

$$E_{\pm}(k_x, k_y) = E_{C(V)} \pm \frac{\hbar^2}{2}\left[\frac{{k_x}^2}{m_{e(h)x}} + \frac{{k_y}^2}{m_{e(h)y}}\right] \quad (1)$$

where E_+ and E_- are electron and hole dispersions, respectively. $E_{C(V)}$ represents conduction (valence) band extrema. $m_{e(h)x}$ and $m_{e(h)y}$, respectively, stand for the electron (hole) effective masses along the x- and y-directions of the device. We have considered x as the transport direction, which in the case of p-type MOSFET, is aligned toward the direction of lower hole effective mass. A schematic of the cross-sectional view of the simulated MOSFET is shown in Figure 3a. First, we discretize the Hamiltonian (1), and then it is fed to the NEGF transport equations, which are solved along with Poisson's equations through a self-consistent loop. We have performed the Poisson-NEGF calculations according to the methodology explained in the work of Brahma et al.[35] First, the electron (hole) correlation function $G^{n(p)}(k_y,E_{\pm})$ is calculated as

$$G^{n(p)}(k_y, E_{\pm}) = G(k_y, E_{\pm})\sum_{n(p)} G^{\dagger}(k_y, E_{\pm}) \quad (2)$$

where $G(k_y,E_{\pm})$ is called the retarded Green's function, which is calculated using the discretized Hamiltonian. We obtain $\sum_{n(p)}$ from in-scattering self-energies due to source and drain contacts. Next, we calculate the carrier density as follows

$$n(p)_q = 2M_v \sum_{k_y} \frac{1}{S}\int_{-\infty}^{+\infty} G^{n(p)}_{q,q}(k_y, E_{\pm})\frac{dE}{2\pi} \quad (3)$$

with $S = L_y \times \Delta x$, where Δx denotes the discretization step along the x-direction and L_y indicates the length of the device in the y-direction. We calculate the current density flowing along the x-direction as follows

$$J^{n(p)}_{q,q+1} = 2M_v \sum_{k_y} \frac{ie^2}{\hbar L_y}\int_{-\infty}^{+\infty} [H_{q,q+1}G^{n(p)}_{q+1,q}(k_y, E_{\pm}) - H_{q+1,q}G^{n(p)}_{q,q+1}(k_y, E_{\pm})]\frac{dE}{2\pi} \quad (4)$$

The value of L_y is taken to be 150 nm, and we have included $n = 30$ uniformly spaced transversal wave vectors, $k_{y,n} = 2\pi n/L_y$, in the computation to satisfy the Born−von Karman periodic boundary conditions in the y-direction of the device. It is assumed that the carrier transport is ballistic, and external metal electrodes form an efficient Ohmic contact with monolayer CP1 borophene. To incorporate spin degeneracy, we have multiplied the whole quantity by a factor of two. In (3) and (4), valley degeneracy (M_v) is equal to 2 for both conduction and valence band extrema, which can be seen in Figure 2c. The self-consistent Poisson-NEGF solver has been accelerated with GPU.[17]

Simulated MOSFET Characteristics. In this section, we explore the device performance of n- and p-type monolayer CP1 borophene MOSFET. For the simulation, we set the device parameters based on the HP (high-performance) specifications from the 2020 edition of the International Roadmap for Devices and Systems (IRDS) for the year 2028. The source and drain extension regions are uniformly doped ($\sim 1 \times 10^{13}$/cm^2), and their lengths (L_S and L_D) are taken to be 30 nm. However, the channel is undoped, and its length (L_{CH}) is the same as the gate length. To investigate the scaling behavior of the transistors, L_{CH} is considered as 10, 7, 5, and 3 nm, where ballistic transport is usually dominant. We set the effective oxide thickness (EOT) and the supply bias (V_{DD}) value to 0.5 nm and 0.65 V, respectively. The thickness of the channel (t_{CH}) is considered equal to the thickness of the monolayer CP1 borophene (2.52 Å) from DFT calculations. The gate work function has been adjusted so that the OFF-state current (I_{OFF}) at zero V_G becomes 10 nA/μm.

Transfer characteristics of n- and p-type MOSFETs for various channel lengths are shown in Figure 3b,c, respectively. The important figures of merit, such as ON-state current (I_{ON}), power delay product (PDP), intrinsic switching delay time (τ), and subthreshold swing (SS) are listed in Table 2. ON current (I_{ON}) is defined as the drain current evaluated at $V_G = V_D = V_{DD}$, where V_D is the drain bias. One of the key figures of merit, subthreshold swing (SS), is defined as the required gate bias to change the subthreshold drain current by one decade, and it should be less than 75 mV/dec as per IRDS requirements.

Nonconvergence of the Poisson-NEGF loop at a higher current value is a well-known problem,[36] and we faced this for L_{CH} = 10 nm devices. The open circles in Figure 3b,c represent the data points where simulations did not converge, and we had to resort to extrapolation. By comparing the behavior of n- and p-type devices, we see that even with the same device configurations, the latter gives a slightly higher I_{ON} than the former. This originates from the fact that carrier injection is predominantly over the barrier at the ON state and the higher density of states of holes, which possess higher effective mass in the y-direction ($m_{ey} = 0.1935\ m_0$ and $m_{hy} = 0.622\ m_0$). Such nearly symmetric (balanced mode) operation of n and p transistors is a very important criterion for complementary metal-oxide semiconductor (CMOS) circuit performance.

We have further studied the energy-resolved current spectrum superimposed on the band edge profile of devices at the OFF state to understand the quantum transport process

https://doi.org/10.1021/acsami.2c20055
ACS Appl. Mater. Interfaces XXXX, XXX, XXX−XXX

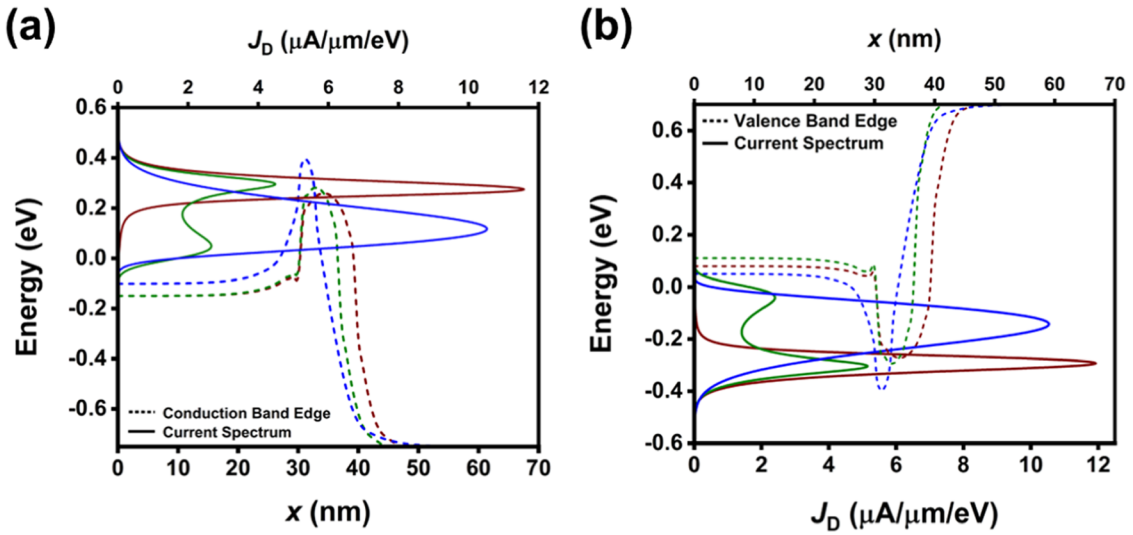

Figure 4. Device characteristics at the OFF state. Energy-resolved current spectrum (J_D) superimposed on (a) conduction band edge profile of n-type and (b) valence band edge profile of p-type MOSFET for L_{CH} = 10, 7, and 3 nm. Here, we use the same color code as Figure 3b,c for the corresponding channel lengths.

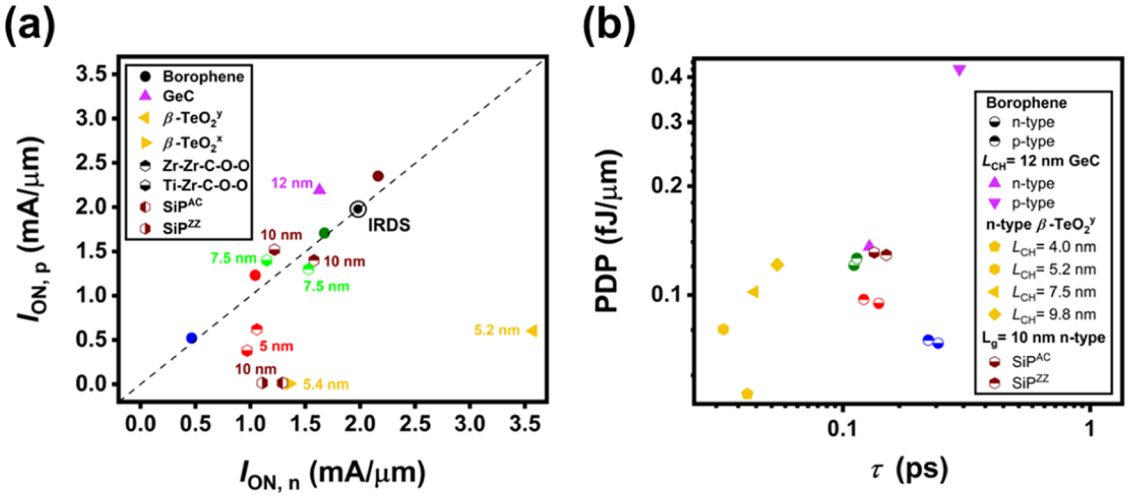

Figure 5. Performance evaluation of n- and p-type transistors. Performance is evaluated (a) in terms of ON-state current (I_{ON}). The I_{ON} for n- and p-type clustered-P1 borophene MOSFET is nicely balanced, especially for L_{CH} = 7 and 3 nm, (b) in the PDP-τ plane against other reported 2D material-based transistors. The superscripts "AC" and "ZZ," respectively, denote the transport direction of transistors along armchair and zigzag directions. L_g indicates the gate length. The superscripts "x" and "y" represent that the transport directions of the device are along the x- and y-directions. The same color code has been used as Figure 3b,c for the corresponding channel lengths of CP1 borophene MOSFET.

(Figure 4). At the OFF state, primarily carriers are thermionically emitted from the source to the channel over the source-to-channel barrier. However, as we scale down L_{CH}, a considerable amount of drain current (I_D) flows under the barrier. This under-the-barrier current component originated due to the quantum mechanical tunneling directly from the source to the drain (shown in Figure S4), leading to the degradation of SS and, hence, I_{ON} for ultrashort channel devices. In Figure 4a,b, it is clearly visible that the peak of the current spectrum is aligned with the top-of-the barrier for L_{CH} = 10 nm, which then gets split into two for L_{CH} = 7 nm, depicting the increase in tunneling current by a considerable percentage. For L_{CH} = 3 nm, severe source-to-drain tunneling occurs, and the current flows far below the top of the source-to-channel barrier. The effective mass responsible for quantum mechanical tunneling is $m_{e(h)x}$ and it is almost equal for electrons and holes (m_{ex} = 0.1935 m_0 and m_{hx} = 0.217 m_0) in this material. As a result, the behavior of current flow and subthreshold slopes are almost similar in n- and p-type MOSFETs (shown in Figure 4a,b, respectively). We have also calculated an average ON-state carrier injection velocity (v_{inj}) at the top-of-the-barrier location (as defined by Klinkert et al.[16]). For n- and p-type devices, the values of v_{inj} are 1.43 × 10^7 and 1.38 × 10^7 cm/s, which are close to the IRDS target value (1.46 × 10^7 cm/s).

Benchmarking Against IRDS and Other 2D Materials. We benchmark the performance of all CP1 borophene devices against the IRDS HP requirements and other 2D material-based devices in terms of ON-state current (I_{ON}), intrinsic switching delay time (τ), and power delay product (PDP). It can be seen in Figure 5a that for 10 and 7 nm channel lengths, I_{ON} is comparable to the IRDS target value (1.979 mA/μm). However, I_{ON} is relatively lower than the target for 5 and 3 nm channel lengths due to direct source-to-drain tunneling. For 3

https://doi.org/10.1021/acsami.2c20055
ACS Appl. Mater. Interfaces XXXX, XXX, XXX−XXX

nm devices, the ON-to-OFF current ratio is observed to be more than 4 decades, which is remarkable. As most of the 2D material-based transistors in the literature are simulated with relaxed OFF current criteria (I_{OFF} = 100 nA/μm), we are able to compare our results with only a few other studies.[17,31−34] The I_{ON} for CP1 borophene MOSFETs is well balanced compared to the transistors based on monolayer β-TeO_2 and SiP; however, the 12 nm monolayer GeC-based transistor shows comparatively balanced I_{ON}. On the other hand, for L_{CH} = 5 nm, I_{ON} of CP1 borophene MOSFET is more nicely balanced than that of Zr−Zr−C−O−O and Ti−Zr−C−O−O Schottky barrier transistors. The switching speed of the transistor is evaluated by intrinsic switching delay time, $\tau = (Q_{ON} - Q_{OFF})/I_{ON}$, where Q_{ON} and Q_{OFF} are the overall mobile charge along the length of the device at ON and OFF states. The power delay product (PDP), calculated as PDP = V_D ($Q_{ON} - Q_{OFF}$), indicates the energy required to switch the transistor. The PDP versus τ plot is shown in Figure 5b. The values of PDP and τ, reported in Table 2, are much lower compared to the IRDS specifications (PDP = 1.003 fJ/μm and τ = 0.78 ps). With decreasing channel length, PDP gradually decreases while τ increases. The PDP and τ of L_{CH} = 7 nm CP1 borophene MOSFET are comparable to n-type 10 nm SiP and 12 nm GeC-based transistors. However, the p-type of GeC-FET possesses a very high value. For 9.8 to 5.2 nm, with decreasing channel length, the n-type β-TeO_2^y transistor shows an opposite trend of τ as compared to our results. With a further decrease in channel length to 4 nm, the trend of τ is the same as our results. However, the reported values of PDP and τ of the 4 nm n-type β-TeO_2^y transistor are much less than those of 3 nm n- and p-type CP1 borophene MOSFET. It is worth mentioning that the transfer characteristics of ultrascaled ($\leq$ 5 nm) devices highly depend on the doping concentration at the source and drain. As shown in Figure S5, higher doping leads to increased source-to-drain tunneling current and hence degradation in SS and I_{ON}. Therefore, the performance of ultrascaled transistors could be further improved by tuning the doping concentration appropriately.

It should be noted that the high contact resistance, which originates from the Schottky nature of the interface between the 2D material and the external metallic circuits, has appeared as the key obstacle for realizing high-performance transistors based on 2D materials. The lack of practical and scalable doping technology for 2D materials has added more difficulties to this problem. In this study, however, we have assumed that the external metal electrodes form an efficient Ohmic contact with monolayer CP1 borophene. Phase engineering[37] and recently proposed functional engineering[17] of 2D materials could be viable options, which naturally offer a metal−metal, low-resistive interface with outside metal wirings. The concept of a phase-engineered borophene transistor, which was proposed earlier by Zhang et al.[18] can also be explored with CP1 borophene. However, we find that among all synthesized metallic polymorphs, only striped borophene possesses a work function (5.56 eV HSE) that can build a Schottky barrier with CP1. Unfortunately, the barrier height is found to be quite large (0.66 eV), which makes the transistor very difficult to switch ON. At the same time, the significant mismatch of lattice constants between the striped and CP1 phases may bring an additional challenge in the experimental realization of such phase-engineered transistors. Other metallic phases may be explored to design high-performance phase-engineered transistors with CP1.

CONCLUSIONS

To conclude, in this study, using evolutionary structure searching, we discovered the clustered-P1 borophene phase, which, in addition to excellent stability, shows ideal material properties for nano transistor applications. Using this allotrope, we propose the possibly lightest conventional MOSFET architecture and simulate its quantum transport properties. By comparing with technology roadmap specifications, we predict that the device is capable of delivering high-performance characteristics even with technology downscaling.

METHODS

DFT Calculations. Primary DFT calculations of this work are carried out using the generalized gradient approximation (GGA) as implemented in the code Vienna Ab initio Simulation Package (VASP)[38−41] with the Projector-Augmented-Wave (PAW)[42] method using the PBE[43] exchange-correlation functional. As discussed before, to address the band gap problem,[26] the band gaps, effective masses, and work functions of all allotropes are determined using the hybrid HSE06 functional.[44] The VASP-supplied B:$2s^2 2p^1$ pseudopotential has been used throughout. A sufficiently large cutoff energy of 520 eV is used to avoid Pulay stress. For all structural relaxations, a Γ-centered k-points grid of $> \frac{45}{a} \times \frac{45}{b} \times 1$ is used to sample the BZ, where a and b are the lattice parameters of the particular cell in Å. A similar k-mesh with a $> \frac{75}{a} \times \frac{75}{b} \times 1$ grid is employed for all static runs, including the HSE ones. Electronic convergence is set to be attained when the difference in energy of successive electronic steps becomes less than 10^{-6} eV, whereas the structural geometry is optimized until the maximum Hellmann−Feynman force on every atom falls below 0.01 eV/Å. A large vacuum space of >25 Å in the vertical direction is applied to avoid any spurious interaction between periodically repeated layers. All crystal structures are visualized using the tool VESTA.[45] The phonon dispersion spectrum was calculated using density functional perturbation theory (DFPT) as implemented in VASP through the code Phonopy[46] with a 2 × 2 × 1 supercell.

Note that here we adopt a combined PBE-HSE workflow to strike a reasonable balance between accuracy and computational efficiency. Properties like structural parameters, dielectric functions, and phonon spectrum require extensive multiple-point calculations, which have not been done at the HSE level. Usually, the PBE prediction is considered accurate enough for these properties.[47] The HSE calculations have been performed only in those cases where a single-point calculation suffices.

The charge partitioning schemes have been applied to the HSE-derived charge density of CP1 borophene. Bader charge analysis was performed using the code developed by the Henkelman group.[48−51] The DDEC6 charge analysis was performed using the Chargemol program (version 3.5) developed by Manz and Limas.[52−54]

Structure Searching. In the 2D limit, a search for the most stable borophene structures is performed using the USPEX code[6,8,20−23] interfaced with VASP, based on an evolutionary algorithm developed by Oganov, Glass, Lyakhov, and Zhu and featuring local optimization, real-space representation, and flexible physically motivated variation operators. Each generated structure's number of atoms is kept between 1 and 10. To keep the systems within the 2D limit, all structures are generated with a 0 Å thickness. At the same time, USPEX allows only the structures with a thickness $\leq$3 Å to remain in contention after a full relaxation, assigning thicker structures a very high positive energy to discourage their generation. This thickness constraint is an extremely crucial parameter and had to be determined empirically from several test runs. One hundred symmetry-constrained random structures are generated for the initial population. In comparison, all subsequent generations contained a population of 100 structures, but with 50% random and 50% inherited structures produced by applying various sophisticated genetic operations on the previous generation's best systems. The search was continued until either 50 generations are completed, or 25 consecutive generations

https://doi.org/10.1021/acsami.2c20055
ACS Appl. Mater. Interfaces XXXX, XXX, XXX−XXX

produce the same results, and it stopped after a total of 37 generations, triggering the latter condition. A 5-fold gradual tightening of DFT parameters is used for this search, the last step following the abovementioned stringent DFT parameters.

AIMD Simulations. For the AIMD simulation of CP1 borophene, a 192-atom supercell was constructed for minimal temperature fluctuations. A canonical ensemble (NVT) is used with a 2 fs timestep, and a Nosé-Hoover thermostat[55,56] is employed with a Γ-point-only *k*-points sampling for the intermediate DFT calculations. The structure was first heated from 0 to 350 K in 2 ps using velocity scaling with an intermediate microcanonical ensemble and subsequently kept at a constant temperature of 350 K for 20 ps.

■ ASSOCIATED CONTENT

Supporting Information

The Supporting Information is available free of charge at https://pubs.acs.org/doi/10.1021/acsami.2c20055.

Crystal structures, bond orders, density of states, and additional device characteristics (PDF)

Video of AIMD of CP1 borophene at 350 K (MP4)

■ AUTHOR INFORMATION

Corresponding Author

Santanu Mahapatra − *Nano-Scale Device Research Laboratory, Department of Electronic Systems Engineering, Indian Institute of Science (IISc) Bangalore, Bangalore 560012, India;* orcid.org/0000-0003-1112-8109; Email: santanu@iisc.ac.in

Authors

Sirsha Guha − *Nano-Scale Device Research Laboratory, Department of Electronic Systems Engineering, Indian Institute of Science (IISc) Bangalore, Bangalore 560012, India;* orcid.org/0000-0002-4330-3971

Arnab Kabiraj − *Nano-Scale Device Research Laboratory, Department of Electronic Systems Engineering, Indian Institute of Science (IISc) Bangalore, Bangalore 560012, India;* orcid.org/0000-0002-7063-0169

Complete contact information is available at: https://pubs.acs.org/10.1021/acsami.2c20055

Author Contributions

S.G. developed and implemented the Poisson-NEGF code, performed simulations of the devices, and analyzed the transistor characteristics. A.K. performed the structure searching and all of the material-related calculations and analyzed the materials data. S.M. conceived the problem statement and supervised the work overall. All authors contributed to writing the manuscript.

Notes

The authors declare no competing financial interest.

■ ACKNOWLEDGMENTS

The research was funded by the Mathematical Research Impact Centric Support (MATRICS) scheme of the Science and Engineering Research Board (SERB), Government of India, under Grant Number MTR/2019/000047.

■ REFERENCES

(1) Ogitsu, T.; Schwegler, E.; Galli, G. *β*-Rhombohedral Boron: At the Crossroads of the Chemistry of Boron and the Physics of Frustration. *Chem. Rev.* **2013**, *113*, 3425−3449.

(2) Tang, H.; Ismail-Beigi, S. Novel Precursors for Boron Nanotubes: The Competition of Two-Center and Three-Center Bonding in Boron Sheets. *Phys. Rev. Lett.* **2007**, *99*, No. 115501.

(3) Mannix, A. J.; Zhou, X.-F.; Kiraly, B.; Wood, J. D.; Alducin, D.; Myers, B. D.; Liu, X.; Fisher, B. L.; Santiago, U.; Guest, J. R.; Yacaman, M. J.; Ponce, A.; Oganov, A. R.; Hersam, M. C.; Guisinger, N. P. Synthesis of Borophenes: Anisotropic, Two-Dimensional Boron Polymorphs. *Science* **2015**, *350*, 1513−1516.

(4) Feng, B.; Zhang, J.; Zhong, Q.; Li, W.; Li, S.; Li, H.; Cheng, P.; Meng, S.; Chen, L.; Wu, K. Experimental Realization of Two-Dimensional Boron Sheets. *Nat. Chem.* **2016**, *8*, 563−568.

(5) Li, W.; Kong, L.; Chen, C.; Gou, J.; Sheng, S.; Zhang, W.; Li, H.; Chen, L.; Cheng, P.; Wu, K. Experimental Realization of Honeycomb Borophene. *Sci. Bull.* **2018**, *63*, 282−286.

(6) Zhou, X.-F.; Dong, X.; Oganov, A. R.; Zhu, Q.; Tian, Y.; Wang, H.-T. Semimetallic Two-Dimensional Boron Allotrope with Massless Dirac Fermions. *Phys. Rev. Lett.* **2014**, *112*, No. 085502.

(7) Lopez-Bezanilla, A.; Littlewood, P. B. Electronic Properties of 8-*Pmmn* Borophene. *Phys. Rev. B* **2016**, *93*, No. 241405.

(8) Zhu, M.-H.; Weng, X.-J.; Gao, G.; Dong, S.; Lin, L.-F.; Wang, W.-H.; Zhu, Q.; Oganov, A. R.; Dong, X.; Tian, Y.; Zhou, X.-F.; Wang, H.-T. Magnetic Borophenes from an Evolutionary Search. *Phys. Rev. B* **2019**, *99*, No. 205412.

(9) Wang, Z.-Q.; Lü, T.-Y.; Wang, H.-Q.; Feng, Y. P.; Zheng, J.-C. Review of Borophene and Its Potential Applications. *Front. Phys.* **2019**, *14*, 33403.

(10) Vishnubhotla, V.; Kabiraj, A.; Bhattacharyya, A. J.; Mahapatra, S. Global Minima Search for Sodium- and Magnesium-Adsorbed Polymorphic Borophene. *J. Phys. Chem. C* **2022**, *126*, 8605−8614.

(11) Salahuddin, S.; Ni, K.; Datta, S. The Era of Hyper-Scaling in Electronics. *Nat. Electron.* **2018**, *1*, 442−450.

(12) Thomas, S. An Industry View on Two-Dimensional Materials in Electronics. *Nat. Electron.* **2021**, *4*, 856−857.

(13) Madhushankar, B. N.; Kaverzin, A.; Giousis, T.; Potsi, G.; Gournis, D.; Rudolf, P.; Blake, G. R.; van der Wal, C. H.; van Wees, B. J. Electronic Properties of Germanane Field-Effect Transistors. *2D Mater.* **2017**, *4*, 021009.

(14) Li, L.; Yu, Y.; Ye, G. J.; Ge, Q.; Ou, X.; Wu, H.; Feng, D.; Chen, X. H.; Zhang, Y. Black Phosphorus Field-Effect Transistors. *Nat. Nanotechnol.* **2014**, *9*, 372−377.

(15) Wang, Y.; Qiu, G.; Wang, R.; Huang, S.; Wang, Q.; Liu, Y.; Du, Y.; Goddard, W. A.; Kim, M. J.; Xu, X.; Ye, P. D.; Wu, W. Field-Effect Transistors Made from Solution-Grown Two-Dimensional Tellurene. *Nat. Electron.* **2018**, *1*, 228−236.

(16) Klinkert, C.; Szabó, Á.; Stieger, C.; Campi, D.; Marzari, N.; Luisier, M. 2-D Materials for Ultrascaled Field-Effect Transistors: One Hundred Candidates under the Ab Initio Microscope. *ACS Nano* **2020**, *14*, 8605−8615.

(17) Guha, S.; Kabiraj, A.; Mahapatra, S. High-Throughput Design of Functional-Engineered MXene Transistors with Low-Resistive Contacts. *npj Comput. Mater.* **2022**, *8*, 202.

(18) Zhang, Y.-L.; Yang, J.-H.; Xiang, H.; Gong, X.-G. Fully Boron-Sheet-Based Field Effect Transistors from First-Principles: Inverse Design of Semiconducting Boron Sheets. *J. Phys. Chem. Lett.* **2021**, *12*, 576−584.

(19) Zhang, J.-J.; Altalhi, T.; Yang, J.-H.; Yakobson, B. I. Semiconducting A′-Boron Sheet with High Mobility and Low All-Boron Contact Resistance: A First-Principles Study. *Nanoscale* **2021**, *13*, 8474−8480.

(20) Oganov, A. R.; Glass, C. W. Crystal Structure Prediction Using Ab Initio Evolutionary Techniques: Principles and Applications. *J. Chem. Phys.* **2006**, *124*, No. 244704.

(21) Oganov, A. R.; Lyakhov, A. O.; Valle, M. How Evolutionary Crystal Structure Prediction Works—and Why. *Acc. Chem. Res.* **2011**, *44*, 227−237.

(22) Lyakhov, A. O.; Oganov, A. R.; Stokes, H. T.; Zhu, Q. New Developments in Evolutionary Structure Prediction Algorithm USPEX. *Comput. Phys. Commun.* **2013**, *184*, 1172−1182.

(23) Wang, Z.; Zhou, X.-F.; Zhang, X.; Zhu, Q.; Dong, H.; Zhao, M.; Oganov, A. R. Phagraphene: A Low-Energy Graphene Allotrope Composed of 5−6−7 Carbon Rings with Distorted Dirac Cones. *Nano Lett.* **2015**, *15*, 6182−6186.
(24) Kabiraj, A.; Bhattacharyya, A. J.; Mahapatra, S. Thermodynamic Insights into Polymorphism-Driven Lithium-Ion Storage in Monoelemental 2D Materials. *J. Phys. Chem. Lett.* **2021**, *12*, 1220−1227.
(25) Penev, E. S.; Bhowmick, S.; Sadrzadeh, A.; Yakobson, B. I. Polymorphism of Two-Dimensional Boron. *Nano Lett.* **2012**, *12*, 2441−2445.
(26) Borlido, P.; Schmidt, J.; Huran, A. W.; Tran, F.; Marques, M. A. L.; Botti, S. Exchange-Correlation Functionals for Band Gaps of Solids: Benchmark, Reparametrization and Machine Learning. *npj Comput. Mater.* **2020**, *6*, 96.
(27) Liu, Y.; Penev, E. S.; Yakobson, B. I. Probing the Synthesis of Two-Dimensional Boron by First-Principles Computations. *Angew. Chem., Int. Ed.* **2013**, *52*, 3156−3159.
(28) Kiraly, B.; Liu, X.; Wang, L.; Zhang, Z.; Mannix, A. J.; Fisher, B. L.; Yakobson, B. I.; Hersam, M. C.; Guisinger, N. P. Borophene Synthesis on Au(111). *ACS Nano* **2019**, *13*, 3816−3822.
(29) Ruan, Q.; Wang, L.; Bets, K. V.; Yakobson, B. I. Step-Edge Epitaxy for Borophene Growth on Insulators. *ACS Nano* **2021**, *15*, 18347−18353.
(30) Smidstrup, S.; Markussen, T.; Vancraeyveld, P.; Wellendorff, J.; Schneider, J.; Gunst, T.; Verstichel, B.; Stradi, D.; Khomyakov, P. A.; Vej-Hansen, U. G.; Lee, M.-E.; Chill, S. T.; Rasmussen, F.; Penazzi, G.; Corsetti, F.; Ojanperä, A.; Jensen, K.; Palsgaard, M. L. N.; Martinez, U.; Blom, A.; Brandbyge, M.; Stokbro, K. QuantumATK: An Integrated Platform of Electronic and Atomic-Scale Modelling Tools. *J. Phys.: Condens. Matter* **2019**, *32*, 015901.
(31) Guo, S.; Qu, H.; Zhou, W.; Yang, S. A.; Ang, Y. S.; Lu, J.; Zeng, H.; Zhang, S. High-Performance and Low-Power Transistors Based on Anisotropic Monolayer -β-TeO_2. *Phys. Rev. Appl.* **2022**, *17*, No. 064010.
(32) Li, Q.; Fang, S.; Liu, S.; Xu, L.; Xu, L.; Yang, C.; Yang, J.; Shi, B.; Ma, J.; Yang, J.; Quhe, R.; Lu, J. Performance Limit of Ultrathin GaAs Transistors. *ACS Appl. Mater. Interfaces* **2022**, *14*, 23597−23609.
(33) Ma, Y.; Dong, L.; Li, P.; Hu, L.; Lu, B.; Miao, Y.; Peng, B.; Tian, A.; Liu, W. First-Principles-Based Quantum Transport Simulations of High-Performance and Low-Power MOSFETs Based on Monolayer Ga2O3. *ACS Appl. Mater. Interfaces* **2022**, *14*, 48220−48228.
(34) Yang, J.; Chen, C.; Zhang, J.; Zhou, W.; Qu, H.; Li, J.; Guo, T.; Shi, X.; Wu, Z.; Zhang, S. High-Performance p-Type 2D FET Based on Monolayer GeC with High Hole Mobility: A DFT-NEGF Study. *Adv. Electron. Mater.* **2022**, *8*, No. 2200388.
(35) Brahma, M.; Bescond, M.; Logoteta, D.; Ghosh, R.; Mahapatra, S. Germanane MOSFET for Subdeca Nanometer High-Performance Technology Nodes. *IEEE Trans. Electron Devices* **2018**, *65*, 1198−1204.
(36) Luisier, M.; Klimeck, G. Atomistic Full-Band Simulations of Silicon Nanowire Transistors: Effects of Electron-Phonon Scattering. *Phys. Rev. B* **2009**, *80*, No. 155430.
(37) Kappera, R.; Voiry, D.; Yalcin, S. E.; Branch, B.; Gupta, G.; Mohite, A. D.; Chhowalla, M. Phase-Engineered Low-Resistance Contacts for Ultrathin MoS2 Transistors. *Nat. Mater.* **2014**, *13*, 1128.
(38) Kresse, G.; Hafner, J. Ab Initio Molecular Dynamics for Liquid Metals. *Phys. Rev. B* **1993**, *47*, 558−561.
(39) Kresse, G.; Hafner, J. Ab Initio Molecular-Dynamics Simulation of the Liquid-Metal–Amorphous-Semiconductor Transition in Germanium. *Phys. Rev. B* **1994**, *49*, 14251−14269.
(40) Kresse, G.; Furthmüller, J. Efficient Iterative Schemes for Ab Initio Total-Energy Calculations Using a Plane-Wave Basis Set. *Phys. Rev. B* **1996**, *54*, 11169−11186.
(41) Kresse, G.; Furthmüller, J. Efficiency of Ab-Initio Total Energy Calculations for Metals and Semiconductors Using a Plane-Wave Basis Set. *Comput. Mater. Sci.* **1996**, *6*, 15−50.
(42) Kresse, G.; Joubert, D. From Ultrasoft Pseudopotentials to the Projector Augmented-Wave Method. *Phys. Rev. B* **1999**, *59*, 1758−1775.
(43) Perdew, J. P.; Burke, K.; Ernzerhof, M. Generalized Gradient Approximation Made Simple. *Phys. Rev. Lett.* **1996**, *77*, 3865−3868.
(44) Heyd, J.; Scuseria, G. E.; Ernzerhof, M. Hybrid Functionals Based on a Screened Coulomb Potential. *J. Chem. Phys.* **2003**, *118*, 8207−8215.
(45) Momma, K.; Izumi, F. *VESTA 3* for Three-Dimensional Visualization of Crystal, Volumetric and Morphology Data. *J. Appl. Crystallogr.* **2011**, *44*, 1272−1276.
(46) Togo, A.; Tanaka, I. First Principles Phonon Calculations in Materials Science. *Scr. Mater.* **2015**, *108*, 1−5.
(47) Wu, K.; Ma, H.; Gao, Y.; Hu, W.; Yang, J. Highly-Efficient Heterojunction Solar Cells Based on Two-Dimensional Tellurene and Transition Metal Dichalcogenides. *J. Mater. Chem. A* **2019**, *7*, 7430−7436.
(48) Tang, W.; Sanville, E.; Henkelman, G. A Grid-Based Bader Analysis Algorithm without Lattice Bias. *J. Phys.: Condens. Matter* **2009**, *21*, No. 084204.
(49) Sanville, E.; Kenny, S. D.; Smith, R.; Henkelman, G. Improved Grid-Based Algorithm for Bader Charge Allocation. *J. Comput. Chem.* **2007**, *28*, 899−908.
(50) Henkelman, G.; Arnaldsson, A.; Jónsson, H. A Fast and Robust Algorithm for Bader Decomposition of Charge Density. *Comput. Mater. Sci.* **2006**, *36*, 354−360.
(51) Yu, M.; Trinkle, D. R. Accurate and Efficient Algorithm for Bader Charge Integration. *J. Chem. Phys.* **2011**, *134*, 064111.
(52) Manz, T. A.; Limas, N. G. Introducing DDEC6 Atomic Population Analysis: Part 1. Charge Partitioning Theory and Methodology. *RSC Adv.* **2016**, *6*, 47771−47801.
(53) Limas, N. G.; Manz, T. A. Introducing DDEC6 Atomic Population Analysis: Part 2. Computed Results for a Wide Range of Periodic and Nonperiodic Materials. *RSC Adv.* **2016**, *6*, 45727−45747.
(54) Manz, T. A. Introducing DDEC6 Atomic Population Analysis: Part 3. Comprehensive Method to Compute Bond Orders. *RSC Adv.* **2017**, *7*, 45552−45581.
(55) Nosé, S. A Unified Formulation of the Constant Temperature Molecular Dynamics Methods. *J. Chem. Phys.* **1984**, *81*, 511−519.
(56) Hoover, W. G. Canonical Dynamics: Equilibrium Phase-Space Distributions. *Phys. Rev. A* **1985**, *31*, 1695−1697.

https://doi.org/10.1021/acsami.2c20055
ACS Appl. Mater. Interfaces XXXX, XXX, XXX−XXX